Continuum states of CO$^+$

N. Vinci and J. Tennyson

Department of Physics and Astronomy, University College London, WC1E 6BT, UK.

Abstract. Continuum states of the CO$^+$ cation are studied as a function of internuclear distances in the range 1.7–3.0 a$_0$. R-matrix wavefunctions are constructed for $^2\Sigma^+$, $^2\Pi$, $^2\Delta$ and $^4\Pi$ total symmetries by study of collisions of electrons with a CO^{2+} target. Complex quantum defects are obtained from above threshold energy scattering calculations yielding resonance energy curves and corresponding electronic couplings to the CO$^+$ continuum. Results are presented and discussed for the high n Feshbach resonances of the CO$^+$ spectrum converging to excited states of CO^{2+}. These curves are responsible for the recently observed dissociative recombination of CO^{2+}.

pacs numbers: 31.15.Ar, 33.15.Bh, 34.10.+x, 34.80.Bm.

1. Introduction

Molecular dications have attracted great interest in recent years. Their formation, structure, decay mechanism and recombination with free electrons in the interstellar medium, in the Earth's upper atmosphere and in the low temperature plasmas formed the subject of many theoretical and experimental studies. Among all these species great attention has been paid to the structure and decay dynamics of the CO^{2+} dication (Mathur 1993, Wetmore et al. 1984, Larsson et al. 1989, Lablanquie et al. 1989, Penent et al. 1998, Safvan et al. 1999, Cossart and Robbe 1999, Andersen et al. 2001, Seiersen et al. 2003). Metastable states of doubly charged molecular ions have been known for many years (Friedlander et al. 1932), but it has been a challenge to characterise experimentally the structure and the peculiar decay mechanism of these molecular species. In spite of the Coulomb repulsion brought by the two positive charges molecular dications can possess long-lived states and it has been only in recent years that well resolved measurements of CO^{2+} metastable state lifetimes have been reported enabling comparison with theory to be made (see, for example, Andersen et al. 1993, Bouhnik et al. 2001, Hinojosa et al. 2002).

Recently, storage ring techniques have also led to a new generation of measurements of dissociative recombination rates for doubly charged ions. The measurements of CO^{2+} dissociative recombination rates, the first for any multiply charged target, were obtained at the ASTRID heavy ion storage ring (Safvan et al. 1999). These measurements were repeated using a corrected calibration formula for the absolute scale of rate coefficients in a more recent experiment (Seiersen et al. 2003). The rates obtained for CO^{2+} at ASTRID are of particular interest for the present study, which provides the *ab initio* curves necessary for a calculation of dissociative recombination (DR) rates in e$^-$ – CO^{2+} collisions. A study based on R-matrix resonance data for NO$^+$ (Schneider et al. 2000) provides the most accurate theoretical model of DR involving a many electron target and the curves reported here should provide the necessary input for a similar study.

Previous theoretical work on CO^{2+} has focussed on its electronic structure. Wetmore et al. (1984) calculated potential curves for CO^{2+} using a restricted [3s,2p,1d] contracted Gaussian basis set and configuration interaction (CI) treatment with self-consistent field (SCF) molecular orbitals (MOs). Correia et al. (1985) employed a larger basis set and a multireference contracted CI (MRCCI) treatment with MOs constructed from complete active space SCF (CASSCF). In an experimental and theoretical study of multiphoton ionisation of carbon monoxide Lablanquie et al. (1989) obtained potential energy curves for the six lowest electronic states. Larsson et al. (1989) employed the same CASSCF/MRCCI methods but with a larger basis set [8s,6p,2d]. These calculations yielded potential energy curves in good overall agreement with the result of Lablanquie et al. (1989). However, discrepancies in the relative position of the lowest electronic states of CO^{2+} showed the need for a more detailed study of this region. Larsson et al.'s (1989) calculations for the $^1\Sigma^+$, $^3\Pi$, $^1\Pi$ and $^3\Sigma^-$ states of CO^{2+} were improved by the calculations of Andersen et al. (1993) who used a larger basis set [8s,5p,3d,1f] and a much larger CI expansion. The agreement between the CASSCF/MRCCI potential curves (Larsson et al. 1989, Andersen et al. 1993) and those of Wetmore et al. (1984) is reasonable for some of the singlet electronic states but, for other states ($^3\Sigma^-$, $^3\Sigma^+$, $2^1\Sigma^+$) the two calculations yield very different results. However, the results obtained by Larsson et al. (1989) and Lablanquie et al. (1989) were in general good agreement with spectroscopy experiments (e.g. Lablanquie et al. 1989, Herman et al. 1987). A detailed comparison between early theoretical investigations can be found in Larsson et al. (1989).

In the present study we use the molecular R-matrix method to provide a description of the e$^-$ – CO^{2+} continuum wavefunctions. Molecular R-matrix theory (Huo and Gianturco 1995) has been used successfully to study the structure and the dynamics of a variety of diatomic and polyatomic molecules and molecular ions (see for example, Tennyson (1996a) and Rabadán and Tennyson (1997)). It provides a framework within which an accurate representation of the molecular system (including electron correlations) can be obtained. This is particularly important for studying the dynamics of collisional systems such as e$^-$ – CO^{2+}, for which accurate wavefunctions of the continuum CO$^+$ states are required. Earlier inner valence and Rydberg state R-matrix calculations for CO$^+$ have been reported (Hayes and Noble 1998). However, in this work low-lying electronic states of CO^{2+} were not accurately reproduced and higher-lying states, including those that are purely dissociative, were not retained in the wavefunction expansion. The only other similar R-matrix calculation to the present one was a study of the continuum states of HeH$^+$ (Tennyson 1998).

In the present work R-matrix wavefunctions for the e$^-$ – CO^{2+} system are calculated. These are used to study the region of the CO$^+$ spectrum where high n Feshbach resonances converge to excited states of CO^{2+}. A CI representation of the lowest seven CO^{2+} target states ($^3\Pi$, $1^1\Sigma^+$, $^1\Pi$, $^3\Sigma^+$, $^3\Sigma^-$, $2^1\Sigma^+$, and $^1\Delta$) are included in the close-coupling expansion. The calculations have been performed for $^2\Sigma^+$, $^2\Pi$, $^4\Pi$ and $^2\Delta$ symmetries. Multichannel Quantum Defect Theory (MQDT) is used to determine the parameters of the Rydberg series.

The outline of the paper is as follows. Following a summary of the molecular R-matrix method, some details are given in section 2 on the approximation that has been adopted and its application to electron scattering calculations for the e$^-$ – CO^{2+} system. CO^{2+} potential energies curves obtained from N-electron wavefunction calculations, the model for CO$^+$ and methods used to determine the resonance parameters are all discussed in this section. Results for CO$^+$ continuum states are presented in section 3. Complex quantum defects obtained from above threshold electron scattering calculations are analysed and results for resonance curves of the CO$^+$ continuum states are discussed. Finally, some conclusions are drawn in section 4.

2. Calculations

A thorough discussion of R-Matrix theory is given by the review of Burke and Berrington (1993) and overviews of its applications to electron collisions with diatomic and polyatomic molecules can be found in Huo and Gianturco (1995) and Tennyson and Morgan (1999). Hence, only a brief summary will be given here.

2.1. The Molecular R-matrix Method

The main assumption in the R-matrix approach is that exchange interactions are negligible when one electron is sufficiently distant from the remaining 'target system'. This leads to a partition of the configuration space into two regions: an internal region where all electron-electron and exchange interactions are fully included, and an external region, in which the outer electron experiences only a local potential. The inner region is defined by a sphere, here taken to have a radius of 10 a_0, about the centre-of-mass of the target.

A set of states Φ_i, usually called target states, are introduced to describe the N-electron molecular target wavefunction. Here the target states are written as a configuration-interaction (CI) expansion of basis configuration ϕ_i by

$$\Phi_i(\mathbf{x}_1...\mathbf{x}_N) = \sum_k c_{ik}\phi_k(\mathbf{x}_1...\mathbf{x}_N) \tag{1}$$

where $\mathbf{x_j} \equiv (\mathbf{r}_j, \sigma_j)$, are the space and spin coordinates of the jth electron and the c_{ik} coefficients are determined by diagonalizing the Hamiltonian H^N of the molecular target in the representation (1). The configurations, ϕ_k, are constructed from target molecular orbitals. The precise choice of these orbitals is important and will be discussed below.

In the internal region the scattering wavefunctions are written as

$$\psi_k = \mathcal{A} \sum_{ij} \Phi_i(\mathbf{x}_1...\mathbf{x}_N)u_{ij}(\mathbf{x}_{N+1})a_{ijk} + \sum_n \chi_n(\mathbf{x}_1...\mathbf{x}_{N+1})b_{kn} \tag{2}$$

where $\mathcal{A}$ is the antisymmetrization operator. The Φ_i are the N-electron target wavefunctions, the u_{ij}, which represent the radial motion of the $(N+1)$th electron, are partial wave expansion about the continuum orbitals. The χ_i are two-center quadratically integrable antisymmetric functions constructed from the target occupied and virtual molecular orbitals. These L^2 functions are included in the (N+1)-electron model to account for charge polarisation (relaxation configurations) and for high ℓ effects near the nuclei (correlation configurations). For diatomic molecules our code (Morgan et al. 1998) uses a linear combination of Slater-type orbitals (STOs) for the target and numerical function to represent the continuum. The coefficients a_{ijk} and b_{kn} are obtained by diagonalising the Hamiltonian of the scattering system in the internal region.

In the external region, the wavefunction is expanded as single-centre solution of close-coupling equations. The only off-diagonal coupling terms are given by the direct potential that is written as a multipole expansion. The internal region is used to define the R-matrix on the boundary. Solutions to the scattering problem are found at infinity by a combination of R-matrix propagation and asymptotic expansion.

2.2. CO^{2+} wavefunctions

All calculations on both CO$^+$ and CO^{2+} were performed for 20 internuclear distances in the range $1.7 - 3.0$ a_0. CO Slater-type orbitals (Kirby-Docken and Liu 1977) were used to build a molecular basis of 44 molecular orbitals (24σ, 14π, 6δ). First, a set of molecular orbitals

Table 1. CO^{2+} vertical energy excitations (in eV) from a 7−state calculation at bond lengths 2.35 and 2.38 a$_0$. These results are given as separations between the $^3\Pi$ state energy at equilibrium geometry and CO^{2+} excited states. Also given the absolute energy of the X $^3\Pi$ state in Hartree and the number of configurations, N. The leading multipole moments, obtained from Natural Orbitals calculations, are given in au.[a]

	N/target−state	CAS+SD[b]	CAS[c]	CASSCF/MRCI[d]	TPEsCO[e]
$R = 2.35$ a$_0$	N(X $^3\Pi$)	49408	496		
	X $^3\Pi$	−111.5580	−111.4871	−111.6517	
	$N(^1\Sigma^+)$	19010	260		
	1 $^1\Sigma^+$	0.193	0.394	0.414	0.373
	2 $^1\Sigma^+$	5.213	5.197		4.123
	$N(^1\Pi)$	32020	352		
	$^1\Pi$	0.607	0.653	0.544	0.522
	$N(^3\Sigma^+)$	28302	297		
	$^3\Sigma^+$	3.393	2.873		2.504
	$N(^3\Sigma^-)$	27519	297		
	$^3\Sigma^-$	2.364	3.072	2.558	
	$N(^1\Delta)$	22376	212		
	$^1\Delta$	4.345	5.224		
	μ(X)	1.3538	1.3178		
	θ(X)	−5.5844	−5.6454		
$R = 2.38$ a$_0$	X $^3\Pi$	−111.5600	−111.4868	−111.6528	
	1 $^1\Sigma^+$	0.239	0.484	0.518	
	2 $^1\Sigma^+$	5.015	5.254		
	$^1\Pi$	0.552	0.654	0.537	
	$^3\Sigma^+$	3.431	2.985		
	$^3\Sigma^-$	2.081	2.838	2.296	
	$^1\Delta$	4.073	4.996		
	μ(X)	1.3540	1.3246		
	θ(X)	−5.6955	−5.7599		

[a] Positive dipoles point from C to O. Note that the sign convention for scattering calculations is used here.
[b] Molecular Orbitals calculations.
[c] Natural Orbitals calculations.
[d] Data adapted from Andersen et al. (1993).
[e] Energies deduced from the TPEsCO spectrum obtained by Dawber et al. (1994).

were obtained by performing calculations from the lowest CO^{2+} SCF states with $^1\Sigma^+$ and $^3\Sigma^-$ symmetries. This SCF molecular basis was then used in CI calculations to obtain 24σ, 14π, 6δ molecular orbitals. In these CI calculations we included all configurations that arise moving 8 electrons in the CAS (3σ,4σ,5σ,6σ,1π,2π) and all single and double excitations from this CAS to the virtual space (7σ-24σ, 3π-14π,1δ-2δ). Such a configuration space yielded low absolute excitation energies, but a large number of configurations (e.g. $\sim$ 50000 for the $^3\Pi$ CO^{2+} state). Use of such target wavefunctions would result in very demanding subsequent scattering calculations. However, the final target Hamiltonian dimensions may be reduced by using pseudo-Natural Orbitals (NOs) to construct the final target wavefunctions, still achieving reliable excitation energies.

To obtained NOs from CI wavefunctions, the original molecular orbitals were transformed using the first order spin reduced density matrix for a given CI state. Hence,
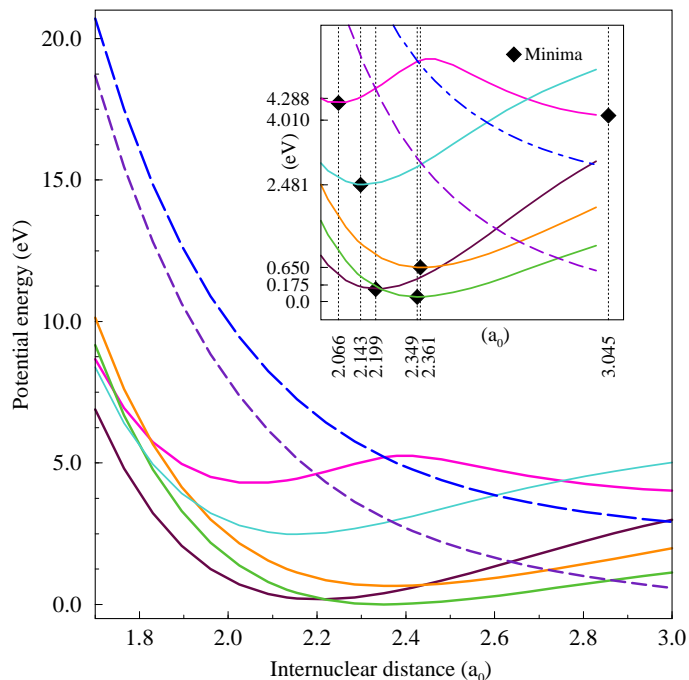
Figure 1. CO^{2+} potential energies curves for the $1\,^1\Sigma^+$ (——), $2\,^1\Sigma^+$ (——), $^3\Pi$ (——), $^1\Pi$ (——), $^3\Sigma^+$ (——), $^3\Sigma^-$ (— — —), and $^1\Delta$ (— —) states.

this new set of averaged NOs was used in further CI calculations to build the final target wavefunctions and compute excitation energies for a 7-state CO^{2+} model. In this model we used 14 natural orbitals, extending the $(3\sigma,4\sigma,5\sigma,6\sigma,1\pi,2\pi)$ valence space to include further 6 NOs $((7\sigma,8\sigma,3\pi,4\pi,1\delta,2\delta)$. The R-matrix molecular computer programs (Morgan et al. 1998, Tennyson and Morgan 1999) that were used for the target wavefunction calculations include SCATCI, DENPROP and PSN (see www.tampa.phys.ucl.ac.uk/rmat). These programs compute CI wavefunctions, density matrices and NOs respectively. Preliminary calculations were performed for few geometries in the vicinity of the equilibrium distance to test the accuracy of our NOs. Results for CO^{2+} electronic excitation energies are summarised in table 1. We compared these data obtained from a CASCI plus electronic excitation calculations and from a CASCI/NOs model with the calculations obtained by Andersen et al. (1993) for the CO^{2+} $^1\Sigma^+$, $^3\Pi$, $^1\Pi$ and $^3\Sigma^-$ states. In general, we find good agreement between the two sets of calculations. Moreover, the CASCI calculations that employ NOs yield a very good result for the separation between the ground $^3\Pi$ state and the first excited states. In our calculations the equilibrium geometry is found to be at an internuclear distance of 2.35 a$_0$. The $^3\Pi$ – $^1\Sigma^+$ separation in this region is less than 0.5 eV and the $^3\Pi$ – $^1\Pi$ separation is about 0.6 eV. The quasi-degeneracy occurring between the three lowest-lying states in the vicinity of the equilibrium distance, is also found in the CASSCF/MRCCI calculations that gave a separation energy between the $^3\Pi$ and the $^1\Sigma^+$ $\leq$ 0.5 eV. The $^3\Pi$ – $^1\Pi$ separation is just above 0.5 eV, with the $^3\Pi$ minimum located at 2.38 a$_0$. In table 1 the energies separations deduced from the threshold photoelectrons coincidence (TPEsCO)

spectrum obtained by Dawber et al. (1994) are also shown; they are in good agreement with our calculations.

The electron properties of CO^{2+} were also investigated. Dipole and quadrupole moments for the X $^3\Pi$ state obtained from CAS+SD and Natural Orbital calculations, are given in table 1. At equilibrium internuclear distance, CO^{2+} dipole moment, $\mu(X)$, is 1.3538 au for the CAS+SD model and 1.3178 au for the CAS model with NOs. The CO^{2+} quadrupole moment, $\theta(X)$, is -5.6844 and -5.6454 au respectively. These values may be compared with those previously obtained for CO^+ and CO. The multipole moments for the X $^2\Sigma^+$ state of CO^+ are discussed in Tennyson (1996a). In this work, $\mu(X)$ varies in the range 0.97 – 1.03 au and $|\theta(X)|$ in the range 1.80 – 1.90 au, depending on the CAS model used in the calculations. Radzig and Smirnov (1985) gave accurate values for $\mu(X)$ and $\theta(X)$ in CO, 0.1098 and -1.5 au respectively. As expected, large (absolute) multipole moments were found in the multiply charged ion. This had to be taken into account in the R-matrix outer region calculations, where the scattered electron moves in the potential induced by target multipole moments.

CO^{2+} potential energy curves for 7-states (1 $^1\Sigma^+$, 2 $^1\Sigma^+$, $^3\Pi$, $^1\Pi$, $^3\Sigma^+$, $^3\Sigma^-$ and $^1\Delta$) used in our calculations are displayed in figure 1. The order of the lowest three states in the vicinity of the equilibrium internuclear separation at 2.35 a_0 is accurately reproduced (inset) as well as the purely dissociative character of the $^3\Sigma^-$ and $^1\Delta$ states. The double minimum that characterises the 2 $^1\Sigma^+$ state is also found. The first minimum is located at 2.07 a_0 and the second one at 3.05 a_0. The second minimum was obtained by extrapolating our 2 $^1\Sigma^+$ data by cubic spline fitting for internuclear distances in the range $3 – 3.1a_0$.

2.3. CO⁺ model

Following Tennyson's (1996a) calculations, we used the 14 CO^{2+} natural orbitals (8σ, 4π, 2δ) to represent the target wavefunctions Φ_i in the close-coupling expansion (2). The target orbitals were augmented by continuum orbitals u_{ij} that were expressed as a truncated partial wave expansion around the centre of mass. Partial waves with $\ell \leq 6$ and $m \leq 2$ were retained in this expansion. The radial part of u_{ij} orbitals are obtained as numerical solutions of an isotropic Coulomb potential. Eigensolutions with an energy below 9.5 Ryd were retained resulting in a set of 63σ, 52π, 42δ continuum functions. To correct for linear dependence effects one σ orbital was removed using Lagrange orthogonalisation (Tennyson et al. 1987). The resulting 62σ, 52π, 42δ functions were Schmidt orthogonalised to the target NOs.

The L^2 functions χ_n in equation 2 were constructed using a CAS comprising the (3σ, 4σ, 5σ, 6σ, 1π, 2π) orbitals. The CAS was augmented by 7-8σ, 3-4π, 1-2δ virtual orbitals. Relaxing configurations were included in the calculations by allocating 9 electrons in the CAS. Correlations configurations arose by allocating 8 electrons in the CAS and 1 electron in the virtual space. This CI model was adopted for all CO^+ total symmeties discussed in this work. The largest CI calculations were performed for the $^2\Pi$ total symmetry. Here, the $^3\Pi$ and $^1\Pi$ target states were coupled with two different partial waves in the close-coupling expansion (2) resulting in a 9-state calculation.

2.4. Resonance characterisation

The CO^{2+} system has several low-lying electronic states which all lie close to each other. This means that even the lowest resonances are narrow with high principal quantum number, n. Furthermore the spacings between these resonances are small.

There are a number of standard procedures for characterising individual resonance states in electron-molecule collision calculations including fitting the eigenphase sum (Tennyson and Noble 1984), the time-delay (Stibbe and Tennyson 1998) and the R-matrix specific QB method (Quigley and Berrington 1996). Extensive numerical investigations suggested that none of these methods, as presently implemented, were capable of yielding stable resonance parameters for this problem. It was therefore necessary to provide an alternative approach.

Multichannel Quantum Defect Theory (MQDT) provides a means of characterising a whole series of resonances as a function of internuclear separation. In this method the portion of the **S**-matrix that belongs to channels of interest, $\mathbf{X_{cc}}$, is diagonalised at an energy just above the threshold to their becoming open (Seaton 1983). For excited state thresholds, this yields complex quantum defects, μ, as eigenvalues with associated eigenvectors, which characterise the partial wave composition of μ. Our procedure is adapted from that used in earlier R-matrix calculations (Tennyson 1988, Tennyson 1996b) of quantum defects in e$^-$ + CH$^+$ and super-excited H$_2$.

In principle each threshold has an infinite number of channels associated with it. In practice, the number of scattering channels that open at each threshold is determined by our choice of partial waves and here is limited to states with $\ell \leq 6$. For $\ell > 6$, $|\mu|$ can be assumed to be very close to zero.

The complex quantum defects obtained by this method in principle characterise the entire resonance series. In practice this method should be most reliable for resonances with high n, such as those studied here. Furthermore, as found previously (Tennyson 1988), the quantum defects provide much the most reliable method of interpolating resonance parameters over a grid of geometries. It should be noted that as we are only concerned with high n states, use of the precise value of the quantum defect makes a relatively small shift in the position of a particular resonance curve. However it is not possible to guess the width of the resonance states simply from a knowledge n.

The accuracy of our scattering calculations, hence of the computed quantum defects and resonance curves, crucially depend on the R-matrix propagation distance. In order to study the stability of results varying this parameter, we computed complex quantum defects for the $^2\Sigma^+$ total symmetry of CO$^+$, using propagation distances in the range $50-1000$ a$_0$. Results from these preliminary calculations, that were performed for CO^{2+} at equilibrium separation, suggested the choice of 400 a$_0$ for the R-matrix propagation radius. This was increased to 500 a$_0$ for calculations with $^2\Pi$ total symmetry.

3. Continuum states of CO$^+$

3.1. Quantum defects analysis

Quantum defects were determined using a scattering energy 0.0008 Ryd above each target state threshold. Sensitivity of results to this choice was studied in preliminary scattering calculations. We obtained quantum defects in CO$^+$ with $^2\Sigma^+$ total symmetry, using above threshold energies in the range $10^{-4} - 10^{-2}$ Ryd and for an energy mesh of 10^{-3} Ryd. Quantum defects from these preliminary tests exhibited differences up to about 10% depending on the above threshold energy. However, for results obtained for above threshold energies in the range $6 \times 10^{-4} - 10^{-3}$ Ryd, these differences decrease to less than 0.1%, suggesting a value of 8×10^{-4} Ryd for our calculations.

This approach yields, for each CO$^+$ total symmetry calculation, a scattering energy grid that varies according to the internuclear distance. Our procedure allows the complex quantum defects obtained from fixed geometry calculations to be organised into curves (Tennyson

1988). Resonance positions $E_{Res}(R)$ and widths $\Gamma_{Res}(R)$ can be computed according to the formulae

$$E_{Res}(R) = E_{Thres}(R) - \frac{Z^2}{\nu^2} \tag{3}$$

$$\Gamma_{Res}(R) = \frac{2Z^2\beta}{\nu^3} \tag{4}$$

where ν is the effective quantum number of the resonance and Z is the ion core electrical charge. This is given by $\nu(R) = n - \alpha(R)$ where n is an integer $\alpha(R)$ is the real part of the complex quantum defect $\mu(R) = \alpha(R) + i\beta(R)$ expressed as a function of the internuclear distance R (Seaton 1983). In eq. (3), $E_{Thres}(R)$ is the target state threshold energy at internuclear separation R.

Table 2: Complex quantum defects (α,β) in e$^-$ - CO^{2+} with $^2\Pi$ total symmetry. Results are displayed for internuclear distances in the range 1.7–3.0 a$_0$ and for the lowest 6 partial waves ($l = 1-6, 0-5$). Power of ten are given in parenthesis for the imaginary component β.

$^1\Sigma^+$

R (a$_0$)/l	1	2	3	4	5	6
. . .						
2.285	0.487, 0.561(-3)	0.367, 0.167(-2)	0.166, 0.491(-1)	0.690, 0.345(-3)	0.985, 0.119(-2)	0.906, 0.372(-2)
2.350	0.260, 0.108(-1)	0.721, 0.184(-1)	0.728, 0.547(-1)	0.032, 0.462(-2)	0.015, 0.883(-4)	1.000, 0.231(-5)
2.380	0.283, 0.519(-2)	0.746, 0.712(-2)	0.974, 0.171(-2)	0.028, 0.181(-3)	0.013, 0.154(-4)	0.997, 0.460(-6)
2.415	0.296, 0.138(-1)	0.619, 0.329(-1)	0.300, 0.225(-3)	0.013, 0.263(-5)	0.998, 0.126(-6)	0.500, 0.580(-12)
2.480	0.451, 0.114(-1)	0.830, 0.723(-2)	0.110, 0.522(-2)	0.028, 0.158(-2)	0.014, 0.967(-3)	0.999, 0.308(-4)
2.545	0.618, 0.328(-1)	0.110, 0.606(-2)	0.945, 0.307(-1)	0.029, 0.110(-2)	0.015, 0.943(-3)	0.100, 0.404(-4)
2.610	0.670, 0.875(-2)	0.146, 0.586(-2)	0.950, 0.417(-2)	0.030, 0.878(-3)	1.000, 0.337(-4)	0.500, 0.240(-14)
2.675	0.387, 0.688(-1)	0.126, 0.572(-1)	0.763, 0.911(-1)	0.728, 0.317(-1)	0.858, 0.272(-1)	0.918, 0.150(-2)
2.740	0.693, 0.578(-1)	0.207, 0.558(-1)	0.101, 0.387(-2)	0.032, 0.799(-3)	0.016, 0.665(-3)	0.000, 0.461(-4)
2.805	0.766, 0.420(-2)	0.950, 0.842(-3)	0.392, 0.634(-1)	0.498, 0.118(-1)	0.500, 0.209(-5)	0.500, 0.115(-11)
2.935	0.195, 0.310(-2)	0.692, 0.213(-2)	0.499, 0.173(-1)	0.081, 0.375(-2)	0.035, 0.271(-3)	0.017, 0.282(-3)
3.000	0.115, 0.539(-1)	0.344, 0.157(-2)	0.179, 0.315(-3)	0.545, 0.110(+0)	0.501, 0.214(-1)	0.500, 0.644(-5)

$2^1\Sigma^+$

R (a$_0$)/l	1	2	3	4	5	6
1.700	0.424, 0.723(-2)	0.612, 0.360(-2)	0.974, 0.407(-2)	0.082, 0.119(-2)	0.045, 0.137(-3)	0.049, 0.200(-3)
1.765	0.314, 0.608(-2)	0.648, 0.436(-1)	0.500, 0.670(-3)	0.012, 0.583(-2)	0.999, 0.548(-3)	0.006, 0.112(-2)
1.830	0.301, 0.906(-2)	0.677, 0.240(-1)	0.058, 0.159(-1)	0.006, 0.287(-2)	0.999, 0.399(-3)	0.500, -0.301(-13)
1.895	0.318, 0.222(-1)	0.501, 0.821(-2)	0.071, 0.069(-1)	0.014, 0.514(-2)	0.007, 0.229(-2)	0.998, 0.448(-3)
1.960	0.326, 0.240(-1)	0.690, 0.141(-1)	0.068, 0.171(-1)	0.996, 0.818(-1)	0.015, 0.541(-2)	0.007, 0.225(-2)
2.025	0.271, 0.102(-1)	0.686, 0.129(-1)	0.069, 0.155(-1)	0.016, 0.483(-2)	0.007, 0.189(-2)	0.997, 0.397(-3)
2.090	0.283, 0.146(-1)	0.702, 0.113(-1)	0.075, 0.145(-1)	0.016, 0.460(-2)	0.008, 0.175(-2)	0.996, 0.353(-3)
2.155	0.604, 0.229(-1)	0.325 0.220(-1)	0.075, 0.178(-1)	0.910, 0.646(-2)	0.996, 0.996(-2)	0.962, 0.377(-4)
2.285	0.086, 0.976(-2)	0.221, 0.228(-2)	0.257, 0.339(-1)	0.648, 0.404(-2)	0.560, 0.110(+0)	0.500, 0.154(-3)
2.350	0.160, 0.130(-4)	0.946, 0.500(-5)	0.195, 0.100(-4)	0.630, 0.130(-4)	0.618, 0.500(-5)	0.878, 0.115(-5)
2.380	0.331, 0.250(-1)	0.705, 0.649(-2)	0.082, 0.843(-2)	0.014, 0.157(-2)	0.007, 0.470(-3)	0.001, 0.709(-4)
2.415	0.698, 0.236(-1)	0.215, 0.338(-1)	0.082, 0.142(-1)	0.014, 0.103(-2)	0.007, 0.320(-3)	0.002, 0.635(-4)
2.480	0.293, 0.613(-2)	0.706, 0.604(-2)	0.095, 0.410(-2)	0.012, 0.452(-3)	0.006, 0.139(-3)	0.002, 0.273(-4)

R (a$_0$)/l					
2.545	0.672, 0.216(-1)	0.279, 0.322(-1)	0.050, 0.132(-1)	0.012, 0.473(-3)	0.006, 0.100(-3)	0.002, 0.192(-4)
2.610	0.321, 0.580(-2)	0.681, 0.853(-2)	0.063, 0.218(-2)	0.013, 0.305(-3)	0.006, 0.940(-4)	0.002, 0.189(-4)
2.675	0.576, 0.124(-1)	0.265, 0.668(-2)	0.166, 0.251(-1)	0.842, 0.439(-1)	0.018, 0.216(-1)	0.946, 0.105(-2)
2.740	0.577, 0.279(-2)	0.259, 0.100(-1)	0.796, 0.550(-2)	0.016, 0.478(-3)	0.007, 0.111(-3)	0.002, 0.222(-4)
2.805	0.613, 0.928(-2)	0.192, 0.760(-2)	0.889, 0.604(-3)	0.972, 0.447(-2)	0.944, 0.172(-3)	0.990, 0.125(-4)
2.935	0.273, 0.185(-1)	0.680, 0.563(-2)	0.061, 0.733(-2)	0.020, 0.597(-3)	0.002, 0.130(-4)	0.010, 0.198(-3)
3.000	0.300, 0.518(-1)	0.677, 0.179(-1)	0.067, 0.333(-2)	0.023, 0.820(-3)	0.011, 0.288(-3)	0.002, 0.284(-3)

$^1\Pi$

R (a$_0$)/l	0	1	2	3	4	5
1.700	0.509, 0.379(-2)	0.250, 0.108(-1)	0.126, 0.206(-1)	0.070, 0.627(-2)	0.969, 0.389(-2)	0.012, 0.181(-2)
1.765	0.494, 0.198(-1)	0.252, 0.127(-1)	0.081, 0.134(-1)	0.074, 0.292(-1)	0.953, 0.145(-1)	0.012, 0.279(-2)
1.830	0.474, 0.369(-1)	0.256, 0.390(-1)	0.806, 0.190(-1)	0.084, 0.206(-1)	0.043, 0.649(-2)	0.021, 0.727(-2)
1.895	0.489, 0.123(-1)	0.251, 0.805(-2)	0.103, 0.125(-1)	0.939, 0.853(-2)	0.063, 0.742(-2)	0.015, 0.152(-2)
1.960	0.499, 0.125(-1)	0.275, 0.110(-1)	0.130, 0.116(-1)	0.913, 0.858(-2)	0.064, 0.772(-2)	0.015, 0.148(-2)
2.025	0.487, 0.156(-1)	0.302, 0.123(-1)	0.144, 0.152(-1)	0.925, 0.737(-2)	0.064, 0.949(-2)	0.016, 0.202(-2)
2.090	0.484, 0.142(-1)	0.500, 0.224(-5)	0.719, 0.158(+0)	0.130, 0.126(+0)	0.122, 0.134(-1)	0.020, 0.295(-2)
2.155	0.456, 0.418(-1)	0.524, 0.993(-1)	0.219, 0.839(-2)	0.923, 0.157(-1)	0.037, 0.645(-2)	0.021, 0.258(-2)
2.285	0.024, 0.272(-1)	0.927, 0.160(-3)	0.437, 0.207(-3)	0.513, 0.219(-5)	0.496, 0.757(-6)	0.503, 0.775(-6)
2.350	0.519, 0.453(-1)	0.381, 0.282(-1)	0.158, 0.146(-1)	0.880, 0.115(-1)	0.019, 0.856(-3)	0.015, 0.458(-2)
2.380	0.448, 0.418(-2)	0.686, 0.301(-1)	0.164, 0.143(-1)	0.881, 0.123(-1)	0.022, 0.947(-3)	0.018, 0.456(-2)
2.415	0.647, 0.384(-2)	0.237, 0.120(-1)	0.490, 0.309(-2)	0.126, 0.793(-1)	0.888, 0.124(-1)	0.500, -0.353(-16)
2.480	0.467, 0.113(-1)	0.500, 0.476(-8)	0.810, 0.233(-2)	0.133, 0.253(-1)	0.906, 0.478(-2)	0.308, 0.146(-2)
2.545	0.450, 0.384(-2)	0.818, 0.473(-3)	0.201, 0.226(-1)	0.923, 0.252(-2)	0.043, 0.293(-1)	0.234, 0.509(-3)
2.610	0.444, 0.990(-2)	0.822, 0.405(-3)	0.144, 0.602(-2)	0.904, 0.430(-2)	0.969, 0.257(-5)	0.290, 0.885(-3)
2.675	0.631, 0.140(-1)	0.659, 0.375(-2)	0.714, 0.538(-3)	0.378, 0.155(-2)	0.362, 0.220(-2)	0.300, 0.481(-2)
2.740	0.443, 0.584(-2)	0.827, 0.174(-2)	0.173, 0.912(-2)	0.926, 0.386(-2)	0.033, 0.521(-2)	0.379, 0.183(-3)
2.805	0.318, 0.900(-2)	0.667, 0.651(-2)	0.056, 0.129(+0)	0.869, 0.152(+0)	0.784, 0.342(-4)	0.804, 0.346(-2)
2.935	0.435, 0.790(-2)	0.814, 0.721(-2)	0.186, 0.147(-1)	0.939, 0.148(-1)	0.946, 0.214(-2)	0.367, 0.647(-3)
3.000	0.420, 0.497(-2)	0.771, 0.179(-2)	0.119, 0.799(-2)	0.922, 0.818(-2)	0.941, 0.117(-2)	0.347, 0.136(-3)

$^1\Delta$

R (a$_0$)/l	1	2	3	4	5	6
1.700	0.645, 0.584(-2)	0.293, 0.790(-2)	0.084, 0.779(-4)	0.988, 0.199(-2)	0.950, 0.397(-4)	0.966, 0.114(-5)
1.765	0.322, 0.612(-2)	0.658, 0.118(-1)	0.085, 0.115(-3)	0.987, 0.137(-2)	0.948, 0.172(-3)	0.966, 0.103(-5)
1.830	0.334, 0.608(-2)	0.654, 0.645(-2)	0.087, 0.118(-3)	0.984, 0.196(-2)	0.951, 0.507(-4)	0.966, 0.114(-5)
1.895	0.277, 0.595(-2)	0.668, 0.135(-1)	0.089, 0.300(-3)	0.993, 0.273(-2)	0.949, 0.208(-3)	0.966, 0.135(-5)
1.960	0.671, 0.202(-1)	0.098, 0.252(-2)	0.076, 0.247(-2)	0.005, 0.366(-2)	0.950, 0.100(-3)	0.966, 0.143(-5)
2.025	0.382, 0.440(-2)	0.658, 0.957(-2)	0.092, 0.225(-3)	0.981, 0.263(-2)	0.953, 0.628(-4)	0.966, 0.175(-5)
2.090	0.402, 0.365(-2)	0.665, 0.865(-2)	0.099, 0.545(-3)	0.033, 0.268(-2)	0.953, 0.763(-4)	0.966, 0.239(-5)
2.155	0.377, 0.542(-2)	0.625, 0.768(-2)	0.071, 0.192(-2)	0.986, 0.457(-2)	0.951, 0.246(-2)	0.965, 0.420(-4)
2.285	0.303, 0.114(-1)	0.157, 0.221(-1)	0.402, 0.289(-1)	0.903, 0.339(-3)	0.718, 0.314(-1)	0.703, 0.887(-3)
2.350	0.551, 0.134(-1)	0.255, 0.135(+0)	0.936, 0.227(-2)	0.105, 0.519(-2)	0.029, 0.711(-3)	0.048, 0.698(-3)
2.380	0.368, 0.808(-2)	0.697, 0.341(-2)	0.104, 0.273(-3)	0.955, 0.104(-3)	0.967, 0.173(-2)	0.967, 0.105(-2)
2.415	0.385, 0.448(-1)	0.733, 0.280(-1)	0.105, 0.945(-3)	0.974, 0.560(-2)	0.954, 0.178(-3)	0.967, 0.447(-4)
2.480	0.314, 0.211(-1)	0.664, 0.324(-1)	0.107, 0.787(-3)	0.950, 0.313(-2)	0.967, 0.305(-4)	0.954, 0.127(-3)
2.545	0.682, 0.156(-1)	0.287, 0.438(-2)	0.177, 0.262(-1)	0.088, 0.628(-2)	0.954, 0.125(-3)	0.967, 0.159(-4)
2.610	0.274, 0.345(-2)	0.687, 0.394(-1)	0.116, 0.624(-1)	0.114, 0.249(-1)	0.954, 0.401(-3)	0.968, 0.954(-4)
2.675	0.903, 0.447(-3)	0.529, 0.459(-1)	0.499, 0.168(-2)	0.500, -0.108(-10)	0.500, 0.670(-11)	0.500, 0.603(-12)
2.740	0.465, 0.197(-1)	0.681, 0.117(-1)	0.118, 0.470(-3)	0.969, 0.402(-4)	0.947, 0.113(-2)	0.953, 0.121(-3)
2.805	0.578, 0.110(-1)	0.221, 0.402(-1)	0.863, 0.246(-2)	0.998, 0.636(-2)	0.925, 0.196(-1)	0.958, 0.989(-3)
2.935	0.669, 0.149(-1)	0.162, 0.137(-1)	0.071, 0.155(-1)	0.013, 0.976(-3)	0.950, 0.168(-3)	0.969, 0.585(-4)
3.000	0.667, 0.130(-1)	0.176, 0.164(-1)	0.079, 0.138(-1)	0.009, 0.568(-2)	0.949, 0.351(-3)	0.970, 0.710(-4)

$^3\Sigma^+$

R (a$_0$)/l	1	2	3	4	5	6
1.700	0.152, -0.105(-9)	0.193, 0.128(-8)	0.948, 0.785(-9)	0.879, -0.168(-8)	0.629, -0.146(-8)	0.616, -0.600(-8)
1.765	0.661, 0.285(-3)	0.179, 0.591(-3)	0.094, 0.506(-4)	0.015, 0.839(-3)	0.966, 0.712(-6)	0.961, 0.121(-5)
1.830	0.340, 0.336(-2)	0.662, 0.925(-3)	0.100, 0.260(-3)	0.013, 0.178(-2)	0.960, 0.963(-4)	0.966, 0.789(-4)
1.895	0.668, 0.360(-2)	0.147, 0.185(-2)	0.100, 0.324(-3)	0.027, 0.270(-2)	0.967, 0.705(-4)	0.960, 0.819(-4)
1.960	0.672, 0.180(-2)	0.128, 0.532(-3)	0.103, 0.259(-3)	0.035, 0.226(-2)	0.967, 0.660(-4)	0.960, 0.729(-4)
2.025	0.346, 0.550(-2)	0.674, 0.231(-2)	0.107, 0.331(-3)	0.020, 0.279(-2)	0.959, 0.674(-4)	0.967, 0.642(-4)
2.090	0.497, 0.196(-1)	0.111, 0.627(-3)	0.040, 0.518(-2)	0.959, 0.643(-4)	0.968, 0.630(-4)	0.500, 0.135(-11)
2.155	0.483, 0.181(-1)	0.638, 0.233(-2)	0.116, 0.550(-3)	0.958, 0.471(-3)	0.966, 0.994(-3)	0.013, 0.194(-2)
2.285	0.377, 0.521(-4)	0.296, 0.165(-2)	0.119, 0.108(-4)	0.597, 0.313(-1)	0.889, 0.428(-2)	0.794, 0.423(-1)
2.350	0.317, 0.101(-1)	0.685, 0.104(-1)	0.120, 0.370(-3)	0.051, 0.316(-2)	0.957, 0.496(-4)	0.969, 0.626(-4)
2.380	0.675, 0.195(-1)	0.155, 0.445(-1)	0.108, 0.409(-2)	0.022, 0.367(-2)	0.955, 0.622(-4)	0.968, 0.545(-4)
2.415	0.680, 0.122(-1)	0.233, 0.391(-1)	0.112, 0.140(-2)	0.024, 0.301(-2)	0.957, 0.518(-4)	0.970, 0.676(-4)
2.480	0.681, 0.393(-2)	0.120, 0.173(-2)	0.019, 0.347(-2)	0.985, 0.459(-1)	0.970, 0.224(-3)	0.956, 0.911(-4)
2.545	0.253, 0.375(-2)	0.683, 0.481(-2)	0.126, 0.706(-3)	0.046, 0.222(-2)	0.956, 0.463(-4)	0.970, 0.582(-4)
2.610	0.683, 0.765(-2)	0.252, 0.581(-2)	0.130, 0.123(-2)	0.053, 0.340(-2)	0.956, 0.481(-4)	0.970, 0.576(-4)
2.675	0.210, 0.634(-2)	0.431, 0.680(-2)	0.540, 0.439(-2)	0.604, 0.311(-1)	0.924, 0.145(-1)	0.963, 0.443(-1)
2.740	0.690, 0.206(-1)	0.213, 0.111(-1)	0.115, 0.139(-2)	0.007, 0.220(-2)	0.955, 0.705(-4)	0.971, 0.716(-4)
2.805	0.502, 0.865(-2)	0.160, 0.186(-1)	0.949, 0.557(-4)	0.918, 0.122(-1)	0.765, 0.453(-2)	0.803, 0.191(-2)
2.935	0.667, 0.100(-1)	0.183, 0.164(-1)	0.109, 0.512(-2)	0.002, 0.331(-2)	0.954, 0.563(-4)	0.971, 0.564(-4)
3.000	0.670, 0.570(-2)	0.199, 0.294(-2)	0.112, 0.629(-3)	1.000, 0.364(-2)	0.954, 0.571(-4)	0.971, 0.463(-4)

$^3\Sigma^-$

R (a$_0$)/l	1	2	3	4	5	6
1.700	0.663, 0.197(-2)	0.291, 0.660(-2)	0.088, 0.891(-4)	0.979, 0.117(-2)	0.951, 0.389(-4)	0.961, 0.408(-6)
1.765	0.312, 0.247(-2)	0.662, 0.376(-2)	0.088, 0.108(-3)	0.982, 0.219(-2)	0.950, 0.147(-3)	0.960, 0.318(-6)
1.830	0.332, 0.516(-2)	0.666, 0.248(-2)	0.091, 0.157(-3)	0.972, 0.195(-2)	0.952, 0.582(-4)	0.961, 0.201(-6)
1.895	0.269, 0.302(-2)	0.669, 0.353(-2)	0.091, 0.139(-3)	0.985, 0.178(-2)	0.951, 0.135(-3)	0.960, 0.486(-6)
1.960	0.673, 0.447(-2)	0.092, 0.195(-2)	0.095, 0.855(-3)	0.996, 0.109(-2)	0.952, 0.881(-4)	0.961, 0.619(-6)
2.025	0.381, 0.432(-2)	0.671, 0.437(-2)	0.095, 0.224(-3)	0.966, 0.181(-2)	0.953, 0.856(-4)	0.961, 0.211(-5)
2.090	0.397, 0.322(-2)	0.676, 0.474(-2)	0.098, 0.313(-3)	0.026, 0.159(-2)	0.953, 0.928(-4)	0.961, 0.358(-5)
2.155	0.271, 0.276(-1)	0.709, 0.269(-1)	0.077, 0.200(-1)	0.019, 0.298(-2)	0.009, 0.140(-2)	0.997, 0.179(-3)
2.285	0.182, 0.155(-2)	0.223, 0.471(-1)	0.746, 0.629(-2)	0.035, 0.598(-2)	0.899, 0.320(-2)	0.500, -0.708(-16)
2.350	0.326, 0.219(-2)	0.700, 0.559(-2)	0.113, 0.181(-2)	0.056, 0.325(-2)	0.953, 0.929(-4)	0.962, 0.208(-4)
2.380	0.342, 0.562(-2)	0.701, 0.231(-2)	0.104, 0.272(-3)	0.954, 0.407(-3)	0.956, 0.489(-3)	0.963, 0.283(-4)
2.415	0.366, 0.580(-2)	0.702, 0.637(-2)	0.103, 0.571(-3)	0.952, 0.796(-3)	0.954, 0.715(-3)	0.963, 0.309(-4)
2.480	0.400, 0.151(-1)	0.744, 0.585(-1)	0.104, 0.461(-2)	0.958, 0.353(-1)	0.952, 0.208(-3)	0.963, 0.327(-4)
2.545	0.285, 0.488(-2)	0.645, 0.508(-1)	0.108, 0.334(-2)	0.002, 0.322(-1)	0.952, 0.480(-3)	0.963, 0.128(-3)
2.610	0.326, 0.345(-1)	0.697, 0.721(-2)	0.118, 0.721(-3)	0.030, 0.224(-2)	0.951, 0.102(-3)	0.964, 0.395(-4)
2.675	0.165, 0.945(-2)	0.245, 0.492(-2)	0.303, 0.654(-1)	0.929, 0.151(-2)	0.655, 0.754(-2)	0.750, 0.299(-2)
2.740	0.451, 0.666(-2)	0.683, 0.611(-2)	0.111, 0.323(-3)	0.937, 0.527(-3)	0.951, 0.874(-4)	0.965, 0.513(-4)
2.805	0.574, 0.302(-1)	0.212, 0.201(-1)	0.857, 0.470(-2)	0.917, 0.301(-1)	0.963, 0.362(-3)	0.954, 0.133(-3)

. . .

$^3\Pi$

R (a$_0$)/l	0	1	2	3	4	5
1.700	0.468, 0.223(-2)	0.182, 0.288(-2)	0.938, 0.121(-2)	0.034, 0.562(-3)	0.012, 0.758(-3)	0.009, 0.479(-4)

1.765	0.618, 0.136(-2)	0.267, 0.171(-2)	0.059, 0.937(-3)	0.027, 0.361(-2)	0.983, 0.951(-3)	0.014, 0.369(-3)
1.830	0.468, 0.193(-2)	0.241, 0.847(-1)	0.167, 0.142(-1)	0.920, 0.127(-2)	0.058, 0.151(-2)	0.030, 0.885(-3)
1.895	0.453, 0.481(-2)	0.190, 0.288(-3)	0.904, 0.228(-2)	0.087, 0.573(-2)	0.011, 0.105(-4)	0.992, 0.168(-3)
1.960	0.443, 0.240(-3)	0.215, 0.792(-3)	0.895, 0.219(-3)	0.065, 0.545(-3)	0.023, 0.654(-3)	0.012, 0.546(-5)
2.025	0.426, 0.103(-2)	0.781, 0.170(-1)	0.134, 0.803(-3)	0.905, 0.208(-2)	0.047, 0.925(-3)	0.014, 0.883(-4)
2.090	0.426, 0.271(-2)	0.205, 0.774(-2)	0.904, 0.239(-2)	0.081, 0.345(-2)	0.970, 0.724(-2)	0.015, 0.713(-4)
2.155	0.497, 0.655(-2)	0.310, 0.689(-2)	0.212, 0.131(-1)	0.879, 0.460(-2)	0.967, 0.999(-3)	0.015, 0.222(-3)
. . .						
2.935	0.399, 0.202(-2)	0.776, 0.394(-3)	0.118, 0.938(-3)	0.900, 0.789(-3)	0.910, 0.605(-3)	0.036, 0.188(-3)
3.000	0.407, 0.662(-2)	0.420, 0.664(-1)	0.795, 0.882(-3)	0.131, 0.231(-2)	0.904, 0.365(-3)	0.057, 0.966(-4)

The energy curve mapping allows a direct reconstruction of the resonance curves converging to each of the CO^{2+} states included in the close-coupling expansion (section 2.3). In eqs. (3) and (4), the resonance energy and width depend on ℓ, the angular momentum quantum number associated with each partial wave. This dependence is carried by the quantum defects $\mu(\mathrm{R})$. As ℓ is not a conserved quantum number, ℓ-labels were assigned to quantum defects according to the norm of their eigenvectors. In most cases this procedure worked well but there are two complicating factors. The first is the fairly large dipole moment of CO^{2+}, which couples the different channels. The second is the frequent curve crossings, see Fig. 1, which is reflected in the quantum defects which also display many (avoided) crossings. In the region of an avoided crossing the ℓ assignment chosen can become somewhat arbitrary. This has to be taken into account when evaluating results presented in table 2 and figs. 2, 3 and 6(a). Inspection of table 2 show a number of cases where β becomes near zero. It is well known that such ultra-long-lived resonances are associated with avoided crossings (Collins et al. 1986).

Complete tables for quantum defects obtained for the CO$^+$ total symmetries discussed in this work are given elsewhere (Vinci 2004). However, quantum defects from a CO$^+$ $^2\Pi$ calculation are given in table 2. This is a representative sample of results that will be discussed in some detail.

Table 2 presents the results of analysing scattering calculations performed 0.0008 Ryd above E$_{\mathrm{Thres}}$. Results are organised in 7 blocks of data, one for each of the target states that were retained in the description of the CO^{2+} wavefunction. Each block of data includes complex quantum defects as a function of the internuclear distance R. Quantum defects are given for the first 6 partial waves ℓ associated with the newly open scattering channels. 'Missing' internuclear distances for some block of data are denoted with dots. These represent geometries for which the parent CO^{2+} electronic state is the ground state and therefore does not give complex quantum defects. For example, those scattering channels opening at the threshold of the $^1\Sigma^+$ target state exhibit complex quantum defects only for distances larger than 2.285 a$_0$, $^1\Sigma^+$ being the lowest state of CO^{2+} for internuclear separation smaller than this. Similarly for the $^3\Pi$ state, complex quantum defects only arise for internuclear distances smaller than 2.155 a$_0$ and larger than 2.935 a$_0$, as it is the lowest state of CO^{2+} for internuclear separation in the region 2.155 – 2.935 a$_0$. A discussion of highly excited bound state of the CO$^+$ ion will be given elsewhere.

In general, it is easier to correlate the low-ℓ quantum defects between geometries than those for high-ℓ which all usually have quantum defects close to zero. However, mixing between ℓ channels is also found in our results for several resonance series and internuclear distances. Strong mixing between quantum defects can yield a failure in attempts to reordering the ℓ assignment using the eigenvector norm analysis. For this reason there are some sets of data in the blocks of table 2 that were not re-ordered by ℓ numbering. This was taken into

account in the construction of the resonance curves presented below.

3.2. Resonances curves for CO$^+$

Resonance curves for the $^2\Pi$, $^2\Sigma^+$, $^2\Delta$ and $^4\Pi$ symmetries are displayed in figures 2 – 7. In order to provide a graphical representation of data adapted from table 2 and from Vinci (2004), complex quantum defects α and β are also shown for some resonance series in the $^2\Pi$ and $^2\Delta$ total symmetries. Resonance curves, energies and widths, were constructed using eqs. (3) and (4). These equations were included in our calculations incorporating the curve mapping procedure discussed in section 3.1 in the existing R-matrix programs for calculations of multichannel quantum defects.

Figures 2 – 7 present resonance widths with only selected values of n. In general, we find that for $n \leq 10$ and internuclear separations larger than the equilibrium distance of 2.35 a$_0$, the (CO$^+$)** curves lie below the ground state of CO^{2+}. For larger n, these curves lie above the CO^{2+} ground state for internuclear separations in the range $1.7 - 3.0$ a$_0$.

Resonance series converging to the $^1\Delta$ state of CO^{2+} are given in figure 2. Complex quantum defects, figure 2(a), can be analysed for the p, d and f partial waves. The real part α generally varies smoothly with internuclear distance and exhibits values in the range 0.1–1.0, the lowest value being associated with the $\ell = 3$, f-wave, and the highest with the d-wave. However, avoided crossings can be noted for some internuclear distances, which result in strong perturbation in both the $\alpha(R)$ and the $\beta(R)$ curves. The imaginary part β varies between 0 and 6×10^{-2} exhibiting fluctuations over the internuclear distance range. Energy curves for resonance series $np\pi$, $nd\pi$, $nf\pi$, with $n = 9, n = 15$ and $n = 20 - 30$ are displayed in figure 2(b), together with the corresponding widths ($n = 9$ and $n = 30$ only). Only curve belonging to high n-series ($n \geq 15$), lie above the CO^{2+} ground state. The behaviour characterising β and its ℓ dependence is reproduced in the resonance widths Γ. However, the magnitude of Γ strongly depend on n: the low-lying series have a maximum width of the order 10^{-2} eV ($n = 9$ in figure 2(b)), while the high-lying series have widths smaller than 10^{-3} eV ($n = 30$ in figure 2(b)).

Figure 3 gives resonance series converging to the purely dissociative $^3\Sigma^-$ state of CO^{2+}. These series present similar features to those discussed for figure 2, where the high-lying resonance converge to the $^1\Delta$ dissociative target state and possess the same π character. Here, the high-lying series cross the $^3\Pi$ ground state of CO^{2+} at large R due to the crossing between the potential energy curves of the $^3\Pi$ and $^3\Sigma^-$ target states. Also there is shift in the the low-lying curves crossing the $^3\Pi$, so that series characterised by $n = 9$ cross the ground state in the vicinity of the equilibrium distance (2.35 a$_0$).

For the $^2\Pi$ symmetry resonances, see figure 4, the resonance curves cross the ground state of CO^{2+} at bondlengths $R < 1.9$ a$_0$, where the $n = 8$ curves lie below the $^3\Pi$ state. All π character series are well above the $^3\Pi$ state for larger internuclear distance and converge to the second excited $^1\Sigma^+$ target state. Strongly varying behaviour is found in the resonance widths that still exhibit differences of one order of magnitude between $n = 8$ and $n = 30$ series. Curves for the $^2\Sigma^+$ total symmetry and for series converging to the $^1\Delta$ target state are displayed in figure 5. Here, the $^1\Delta$ state is coupled with the δ continuum in the construction of the $^2\Sigma^+$ CO$^+$ wavefunction, so that contributions due to the $\ell = 2 - 4$ partial waves can be distinguished in the graphs. In particular, low-lying $nd\delta$ curves cross the $^3\Pi$ ground state in the vicinity of the equilibrium distance while the high-lying resonances ($n \geq 13$) lie above the ground state for all internuclear separations in the range 1.7–3.0 a$_0$.

Complex quantum defects and resonance curves of the $^2\Delta$ total symmetry in CO$^+$ are presented in figure 6(a) and 6(b). For $n \geq 15$ the $ns\sigma$, $np\sigma$, $nd\sigma$ resonance series lie above
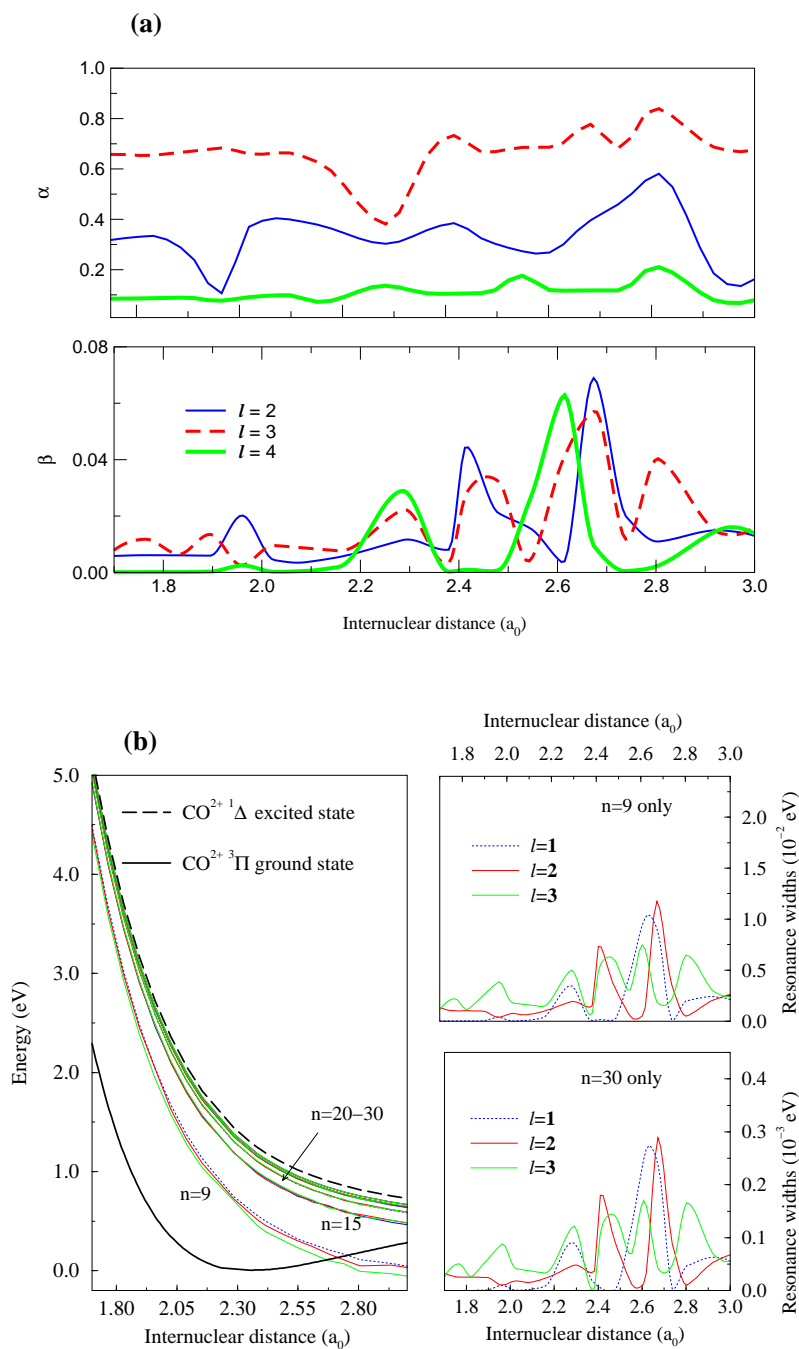
Figure 2. (a) Complex quantum defects (α, β) for the $^2\Pi$ total symmetry and for series converging to the CO^{2+} $^1\Delta$ state. (b) Resonance positions (Energy) and widths (Γ) for the same total symmetry and resonance series.
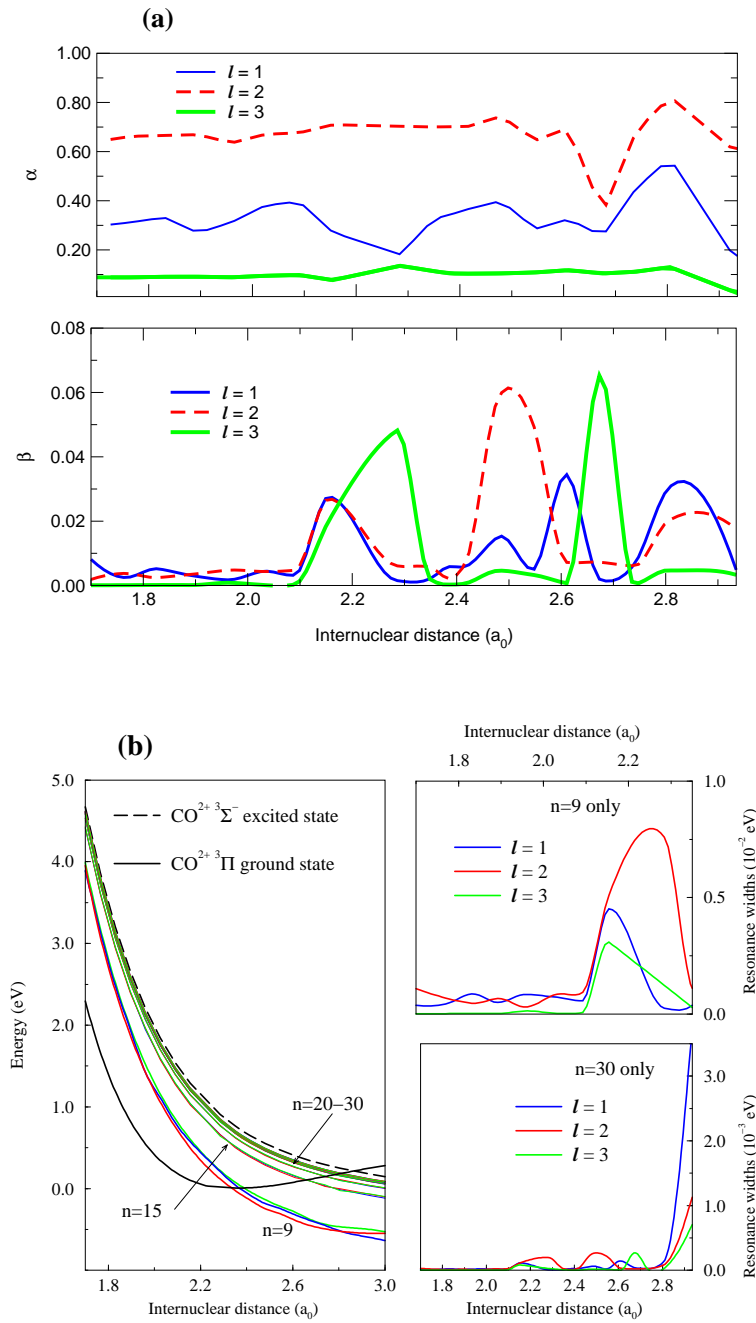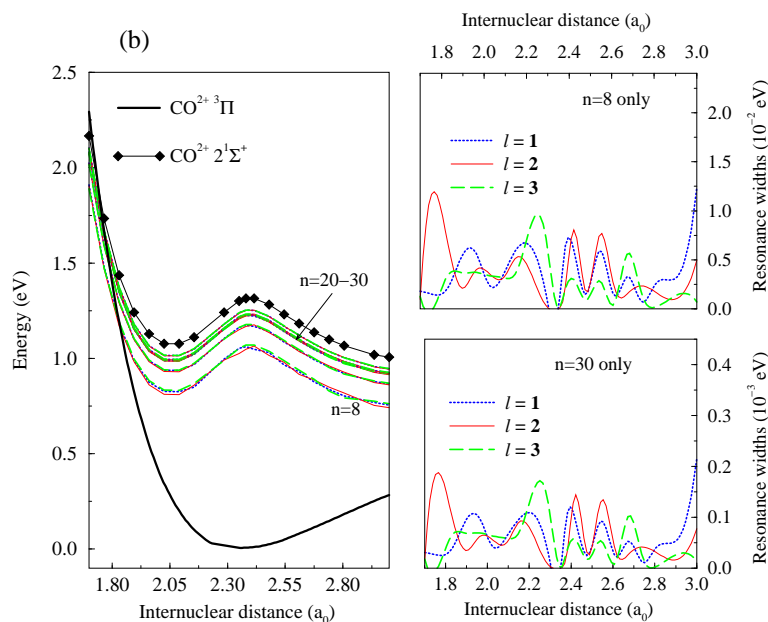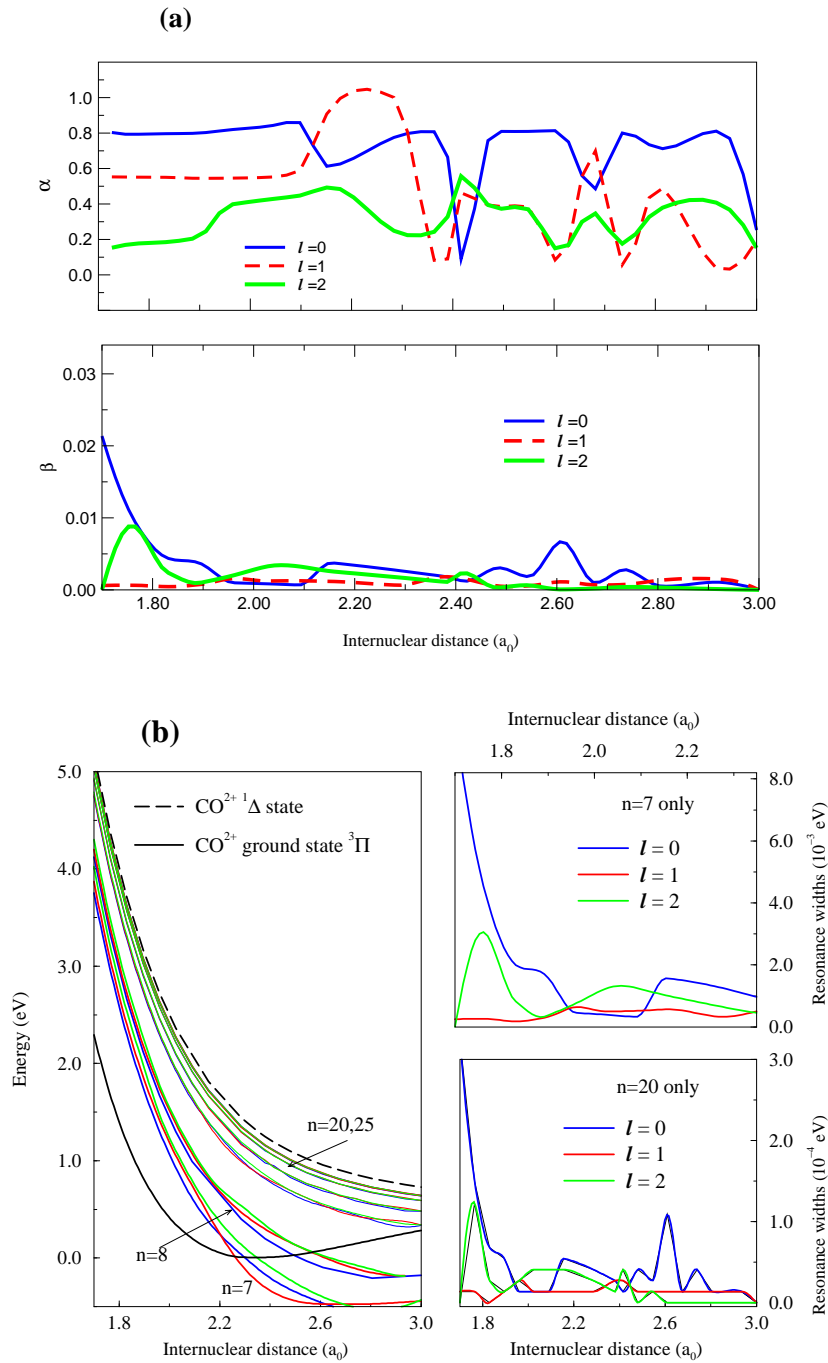
(a)

(b)

Figure 3. **(a)** Complex quantum defects (α, β) for the $^2\Pi$ total symmetry and for series converging to the CO^{2+} $^3\Sigma^-$ state. **(b)** Resonance positions (Energy) and widths (Γ) for the same total symmetry and resonance series.

Figure 4. Resonance positions (Energy) and widths (Γ) for the $^2\Pi$ total symmetry and for resonance series converging to the CO^{2+} $2\,^1\Sigma^+$ state.
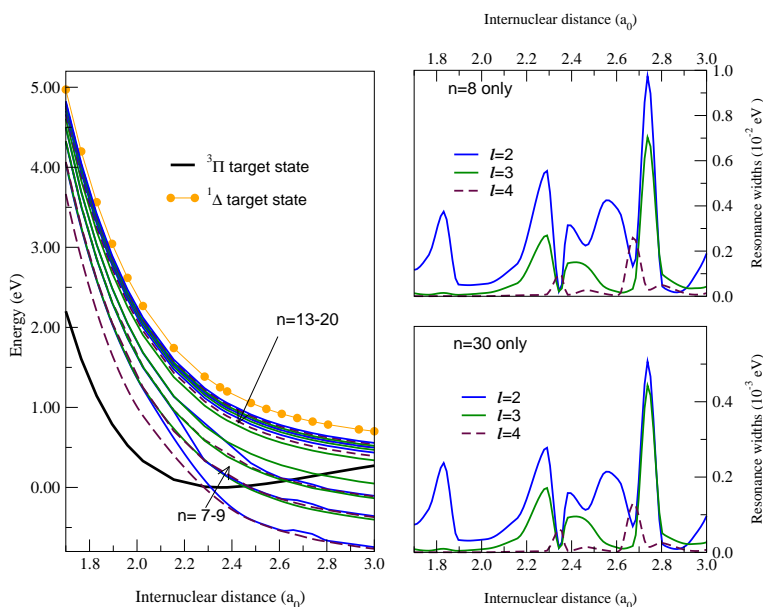
Figure 5. Resonance positions (Energy) and widths (Γ) for the $^2\Sigma^+$ total symmetry for series converging to the CO^{2+} $^1\Delta$ state.

the ground state of CO^{2+}. High-lying series converge to the $^1\Delta$ target state for $n \geq 20$. These σ resonances exhibit smaller widths than the π resonances discussed above: the $7s\sigma$,

Figure 6. **(a)** Complex quantum defects (α, β) for the $^2\Delta$ total symmetry and for series converging to the CO^{2+} $^1\Delta$ state. **(b)** Resonance positions (Energy) and widths (Γ) for the same total symmetry and resonance series.

.

$7p\sigma$ and $7d\sigma$ and $20s\sigma$, $20p\sigma$ and $20d\sigma$ resonance series have widths $0 \leq \Gamma \leq 8 \times 10^{-3}$ and $0 \leq \Gamma \leq 3 \times 10^{-4}$ respectively.

Finally we discuss the continuum states for the CO^+ $^4\Pi$ symmetry. A π character is assigned to the series presented in figure 7. These high-lying curves converge to the $^3\Sigma^-$ target state. The $40p\pi$ energy curve in figure 7 is well below the $^3\Sigma^-$ potential energy with a maximum distance of 0.75 eV from the target state curve. Resonance widths are two orders of magnitude smaller than the π resonances in the CO^+ $^2\Pi$. We found resonance widths $0 \leq \Gamma \leq 8 \times 10^{-4}$ and $0 \leq \Gamma \leq 4 \times 10^{-5}$ for the $15p\pi$, $15d\pi$, $15f\pi$ and $40p\pi$, $40d\pi$, $40f\pi$ series respectively. The behaviour of Γ as a function of internuclear distance is also different: the smooth dependence of Γ on R is broken by a large structure only in the region 2.4–2.6 a_0. This is almost certainly due to the fact that quartet symmetries do not couple to the CO^{2+} singlet target states thus greatly reducing the number of (possible) avoided crossings.
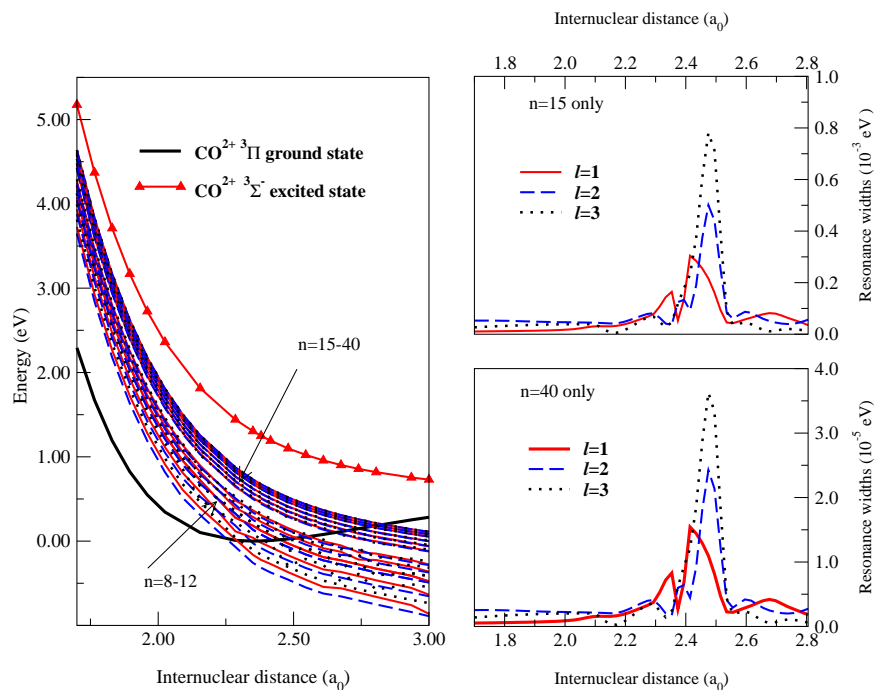

Figure 7. Resonance positions (Energy) and widths (Γ) for the $^4\Pi$ total symmetry for series converging to the CO^{2+} $^3\Sigma^-$ state.

.

4. Conclusions

Ab initio curves for the CO^+ continuum states of symmetries $^2\Sigma^+$, $^2\Pi$, $^2\Delta$ and $^4\Pi$ have been calculated using the R-matrix method. Curves for the very many low energy resonances, which are potentially important for dissociative recombination of CO^{2+}, have been constructed from calculated complex quantum defects. The relevent quantum defects were obtained from above threshold energy scattering calculations performed for internuclear distances well outside the region of CO^+ and CO^{2+} equilibrium separations.

The exceptionally high density of low-lying Rydberg states in CO^{2+} meant that the use of a Multichannel Quantum Defect Theory (MQDT) approach to the e$^-$ + CO^{2+} resonance problem was the only one practical. Using this approach, data for quantum defects in CO$^+$ have been obtained for 20 internuclear distances in the range 1.7 –3.0 a$_0$. Following an analysis of complex quantum defect structure, resonance curves were discussed providing data and graphs for representative series in the $^2\Sigma^+$, $^2\Pi$, $^2\Delta$ and $^4\Pi$ symmetries of CO$^+$.

Using our CO$^+$ wavefunctions, a study of bound Rydberg states of this system can be performed over a large range of internuclear distances complementing the present study on the e$^-$ + CO^{2+} scattering system. Moreover, this work provides *ab initio* data for further studies on the dissociative recombination of CO^{2+}. Calculations for dissociative recombination rates of CO^{2+} will allow a direct comparison with experiment and a better insight of the recombination mechanism in molecular doubly-charged ions.

Acknowledgements

References

Andersen L H, Posthumus J H, Vahtras O, Ågren H, Elander N, Nunez A, Scrinzi A, Natiello M and Larsson M 1993 *Phys. Rev. Lett.* **71**, 1812–1815.

Andersen T, Kjeldsen H, Knudsen H and Folkmann F 2001 *J. Phys. B: At. Mol. Opt. Phys.* **34**, L327.

Bouhnik J P, Gertner I, Rosner B, Amitay Z, Heber O, Zajfman D, Sidky E Y and Ben-Itzhak I 2001 *Phys. Rev. A* **63**, 032509.

Burke P G and Berrington K A, eds 1993 *Atomic and Molecular Processes: An R-matrix approach* Bristol and Philadelphia: Institute of Physics Publishing.

Collins L A, Schneider B I, Noble C J, McCurdy C W and Yabushita S 1986 *Phys. Rev. Lett.* **57**, 980–983.

Correia N, Flores-Riveros A, Ågren H, Helenelund K, Asplund L and Gelius U 1985 *J. Chem. Phys.* **83**, 2035.

Cossart D and Robbe J M 1999 *Chem. Phys. Lett.* **311**, 248–254.

Dawber G, McConkey A G, Avaldi L, MacDonald M A, King G C and Hall R I 1994 *J. Phys. B: At. Mol. Opt. Phys.* **27**, 2191–2209.

Friedlander E, Kallman H, Lasereff W and B.Rosen 1932 *Z. Physik* **76**, 60.

Hayes M A and Noble C J 1998 *J. Phys. B: At. Mol. Opt. Phys.* **31**, 3609–3619.

Herman Z, Jonathan P, Brenton A G and Beynon J H 1987 *Chem. Phys. Lett.* **141**, 433.

Hinojosa G, Covington A M, Phaneuf R A, Sant'Anna M M, Hernandez R, Domínguez I, Bozek J D, Schlachter A S, Alvarez I and Cisneros C 2002 *Phys. Rev. A* **66**, 32718.

Huo W M and Gianturco F M, eds 1995 *Computational Methods for Electron-Molecule Collisions* New York:Plenum.

Kirby-Docken K and Liu B 1977 *J. Chem. Phys.* **66**, 4309.

Lablanquie P, Delwiche J, Hubin-Franskin M J, Nenner I, Morin P, Ito K, Eland J H D, Robbe J M, Gandara G, Fournier J and Fournier P G 1989 *Phys. Rev. A* **40**, 5673.

Larsson M, Olsson B J and Sigray P 1989 *Chem. Phys.* **139**, 457–469.

Mathur D 1993 *Phys. Rep.* **225**, 193.

Morgan L A, Tennyson J and Gillan C J 1998 *Computer Phys. Comms.* **114**, 120–128.

Penent F, Panajotović R I, Eland J H D, Chaplier G and Lablanquie P 1998 *Phys. Rev. Lett.* **81**, 3619.

Quigley L and Berrington K A 1996 *J. Phys. B: At. Mol. Phys.* **29**, 4529–4542.

Rabadán I and Tennyson J 1997 *J. Phys. B: At. Mol. Opt. Phys.* **30**, 1975–1988. erratum 31, 4485-4487 (1998).

Radzig A A and Smirnov B M, eds 1985 *Reference Data on Atoms, Molecules, and Ions* Springer-Verlag Berlin Heidelberg.

Safvan C P, Jensen M J, Pendersen H B and Andersen L H 1999 *Phys. Rev. A* **60**, R3361.

Schneider I F, Rabadán I, Carata L, Tennyson J, Andersen L H and Suzor-Weiner A 2000 *J. Phys. B: At. Mol. Opt. Phys.* **33**, 4849–4861.

Seaton M J 1983 *Rep. Prog. Phys* **46**, 167.

Seiersen K, Heber O, Jensen M J, Safvan C P and Andersen L H 2003 *J. Chem. Phys.* **119**, 839.

Stibbe D T and Tennyson J 1998 *Computer Phys. Comms.* **114**, 236–242.

Tennyson J 1988 *J. Phys. B: At. Mol. Opt. Phys.* **21**, 805–816.

Tennyson J 1996*a J. Phys. B: At. Mol. Opt. Phys.* **29**, 6185–6201.

Tennyson J 1996*b At. Data Nucl. Data Tables* **64**, 253–277.

Tennyson J 1998 *J. Phys. B: At. Mol. Opt. Phys.* **31**, L177–L185.

Tennyson J, Burke P G and Berrington K A 1987 *Computer Phys. Comms.* **47**, 207–212.

Tennyson J and Morgan L A 1999 *Phil. Trans. A* **357**, 1161–1173.

Tennyson J and Noble C J 1984 *Computer Phys. Comms.* **33**, 421–424.

Vinci N 2004. `http://www.tampa.phys.ucl.ac.uk/moldata`.

Wetmore R W, LeRoy R J and Boyd R K 1984 *J. Phys. Chem.* **88**, 6318–6328.